






# Classification of Biological Scatters Using Polarimetric Weather Radar

Cheng Hu , Senior Member, IEEE, Zhuoran Sun , Kai Cui , Huafeng Mao , Rui Wang , Xiao Kou, Dongli Wu, and Fan Xia

**Abstract**—Weather radar holds the capability to monitor the extensive migration of bird and insect species. In particular, polarimetric weather radar can enhance aerial ecological monitoring by quantifying target shape through the measurement of polarization moments. This article introduces an intelligent algorithm to classify bird and insect migration using polarimetric weather radar data. A radar image dataset was formed by intentionally curating typical migratory data of birds and insects captured by the polarimetric weather radar. Next, point features and spatial texture features were extracted from the radar images in the dataset for training a classifier using a supervised learning approach, resulting in a classification accuracy of 93.56%. Furthermore, the importance of the features was analyzed, uncovering that the most influential attribute was the reflectivity factor at 33.83%, surpassing the cumulative influence of other dual-polarization moments. In addition, spatial textures also played an essential role for the classifier, collectively weighing 35.65%. Lastly, the proposed method was validated with bird radar data, attaining an accuracy level of 95.36%.

**Index Terms**—Biological scatters classification, bird migration, bird radar, polarimetric weather radar, random forest.

## I. INTRODUCTION

EVERY year, hundreds of millions of insects, birds, and bats migrate over long distances between their breeding and overwintering grounds [1]. Animal migration is a complex phenomenon that affects various aspects of ecosystem functions, processes, and biogeochemistry [2]. However, in recent years,

changes in global phenology and the environment have resulted in a significant decline in the populations of birds and insects [3], [4]. Furthermore, migrant animals have a close relationship with human life. Insect pest migration can inflict substantial damage to crops, while the migration of birds and bats can lead to epidemics of human and animal diseases [5], [6].

Located in the East Asian monsoon climate zone, China provides a stable background field of wind and temperature for the seasonal migration of insects, which is widespread in eastern China [7], [8]. In late spring and early summer, 119 species of insects in northern China enter and exit the northeast agricultural area through the Bohai Bay migratory channel with the East Asian monsoon, accounting for more than 90% of the total biomass in the northeast region of China [9]. China is a crucial avian migration channel in the world, with birds traveling long distances within its borders. Three of the world's eight bird migration routes pass through China [10]. Effective monitoring is necessary to further study the migration behavior of animals. Weather radars are powerful observation instruments for studying large-scale biological migration due to their long detection range and the ability to work continuously day and night [11], [12]. By analyzing massive weather radar data, researchers can assess the response of migratory animals to climate change and interpret macroecological laws [13], [14].

Monitoring biological migration using weather radars requires the retention of biological echoes and the removal of precipitation echoes. Numerous researchers have contributed to this field [15], [16], [17], [18]. Biological echoes can be divided into birds, bats, and insects, and the correct classification of these echoes can improve the accuracy of quantifying migratory biomass [19], [20]. The traditional method for classifying mass migration of birds, bats, and insects generally uses a threshold based on their velocity features. Dokter et al. [11] used the volume velocity profiling method to calculate the  $\sigma_r$  (standard deviation of the fit residuals of radial velocity) of migratory animals, classifying animals with  $\sigma_r$  greater than 2 m/s as birds and those with  $\sigma_r$  less than or equal to 2 m/s as insects. Nussbaumer et al. [21] counted the airspeed and  $\sigma_r$  of birds and insects, respectively, and used a Gaussian mixture model to fit the two parameters and estimate the mixing ratio of birds and insects. However, using the velocity features of birds (bats), and insects to classify them has limitations. Calculating the airspeed of migratory animals requires estimating their ground speed and subtracting the wind speed. Methods for calculating the ground speed of migratory animals using weather radars generally

Manuscript received 2 September 2023; revised 1 March 2024; accepted 13 March 2024. Date of publication 19 March 2024; date of current version 3 April 2024. This work is supported in part by the National Natural Science Foundation of China under Grant 62225104 and Grant 62301048, and in part by the Shandong Provincial Natural Science Foundation under Grant ZR2023QF035. (Corresponding author: Kai Cui.)

Cheng Hu, Zhuoran Sun, Kai Cui, Huafeng Mao, Rui Wang, and Xiao Kou are with the Radar Technology Research Institute and School of Information and Electronics, Beijing Institute of Technology, Beijing 100081, China, also with the Key Laboratory of Electronic and Information Technology in Satellite Navigation, Beijing Institute of Technology, Ministry of Education, Beijing 100081, China, and also with the Advanced Technology Research Institute, Beijing Institute of Technology, Jinan 250300, China (e-mail: hucheng.bit@gmail.com; szr@bit.edu.cn; bitcui kai@gmail.com; huafengmao@163.com; wangrui.bit@bit.edu.cn; kou-xiao\_0406@163.com).

Dongli Wu is with the Meteorological Observation Center of China Meteorological Administration, Beijing 100081, China (e-mail: wudongli666@126.com).

Fan Xia is with the Key Laboratory for Meteorological Disaster Prevention and Mitigation of Shandong Province, Jinan 250031, China, and also with the Shandong Institute of Meteorological Sciences, Jinan 250031, China (e-mail: xf0718@126.com).

Digital Object Identifier 10.1109/JSTARS.2024.3378801

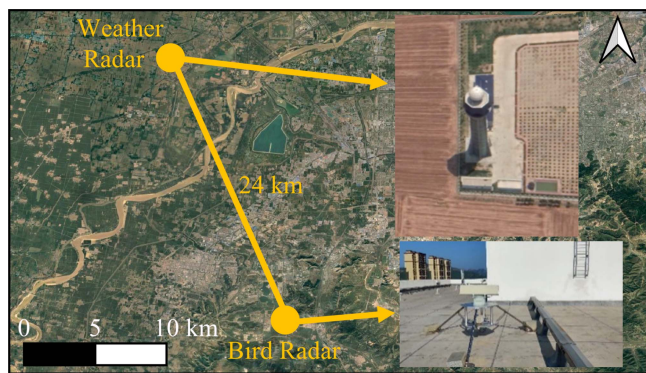


Fig. 1. Geographical coordinates of the polarimetric weather radar and the bird radar.

require every azimuth angle in the same range gate to have echoes during an azimuth scan [22]. If some azimuths lack echoes, the calculated error of their ground speed will increase, with the error growing larger as more echoes are missed. Additionally, the spatial resolution of these methods has limitations, because it cannot classify birds and insects individually for each range bin on a plan position indicator (PPI) image of weather radars.

Methods of using polarization moments to classify birds and insects have been developed with the increasing popularity of polarimetric weather radars. Stepanian et al. [23] conducted an analysis of the polarization moments of birds and insects, respectively, and discovered a significant difference in the polarization moments between the two groups. Jatau et al. [24], [25] utilized WSR-88D dual-polarization data to train several classifiers based on fuzzy logic algorithm, ridge regression classification, and the decision tree method. The resolution unit of classifiers was one range bin, and the classification accuracy of classifiers was more than 85%. Gauthreaux and Diehl [26] employed the random forest algorithm to classify birds, insects, and precipitations, and achieved a classification accuracy of more than 92%. In summary, the existing methods for classifying the migration of birds and insects based on airspeed and  $\sigma_r$  have some limitations, such as low spatial resolution, relatively low accuracy, and lack of verification methods. The existing polarization classification methods have addressed the issue of low spatial resolution, yet ample opportunities exist for enhancing classifier performance by incorporating spatial textures of radar moments. Furthermore, a majority of prevailing methodologies were tailored for the next generation weather radar or the operational program for the exchange of weather radar information. Nonetheless, scant research has been conducted on classification methods for biological scatterers using the China New Generation Weather Radar Network (CINRAD).

This article establishes a radar image dataset of migratory animals acquired by the polarimetric weather radar situated at the Jinan site. A classifier for biological scatterers, utilizing the point features and spatial texture features from the radar image dataset, is trained to classify bird and insect migrations, achieving an accuracy rate of 93.56%. The investigation examines the impact

of six distinct types of polarimetric weather radar moments and their spatial textures on classifier performance. The reflectivity factor emerges as the most dominant moment affecting classifier performance, contributing to 33.83% of the overall influence. Spatial textures also played a crucial role for the classifier, collectively accounting for 35.65%. Five representative scenarios, encompassing two bird cases, two insect cases, and a combined case of birds and insects, validate the performance of the biological scatterer classifier. In addition, a bird radar is employed to both verify and assess the performance of the biological scatter classifier. The labels generated by the bird radar serve as the ground truth and are compared with those generated by the biological scatterer classifier, resulting in an accuracy of 95.36% and confirming the strong performance of the biological scatterer classifier.

## II. MATERIALS

Shandong province is the important migration channel for aerial animals, many migration birds and insects are passing through here and cross the Bohai Bay [27], [28]. Therefore, the polarimetric weather radar located in Jinan city, Shandong province, China, is selected as the data source for our method. The proposed method is verified and evaluated through a joint observation experiment with weather radars and a phased array bird radar.

### A. Weather Radar

CINRAD has established over 200 weather radars in central and eastern China. The S-band polarimetric weather radar used in this article is situated in Jinan city, Shandong province, China, at east longitude  $116^{\circ}43'$  and north latitude  $36^{\circ}43'$ , as illustrated in Fig. 1.

Through manual inspection of polarimetric weather radar data from the Jinan site, we discerned two distinct categories of biological echoes. Type I echoes demonstrate a pronounced azimuthal correlation in their differential reflectivity and differential phase. These echoes predominantly manifest during nighttime hours spanning (from sunset to sunrise of next day) from April to June or August to November, as illustrated in Fig. 2. In contrast, type II echoes lack substantial fluctuations in differential reflectivity and differential phase relative to the azimuth angle. These echoes predominantly emerge during daylight hours spanning from March to November (from sunrise to sunset) and during nighttime in July, as depicted in Fig. 3. In summary, type I echoes are likely dominated by birds (potentially including some bats), while type II echoes are dominated by insects [23], [24], [29]. Based on the aforementioned characteristics, we manually annotated the weather radar image to construct a dataset encompassing migratory flying animals.

Given the variations in seasonal animal migration intensity, the labeled data must encompass spring, summer, and autumn to ensure data comprehensiveness. Weather radar data from the Jinan site during spring (April, May), summer (July), and autumn (September, October) of 2021 were chosen as the foundational source for the migratory flying animal dataset. The  $2.4^{\circ}$  elevation angle PPI image was employed for training and

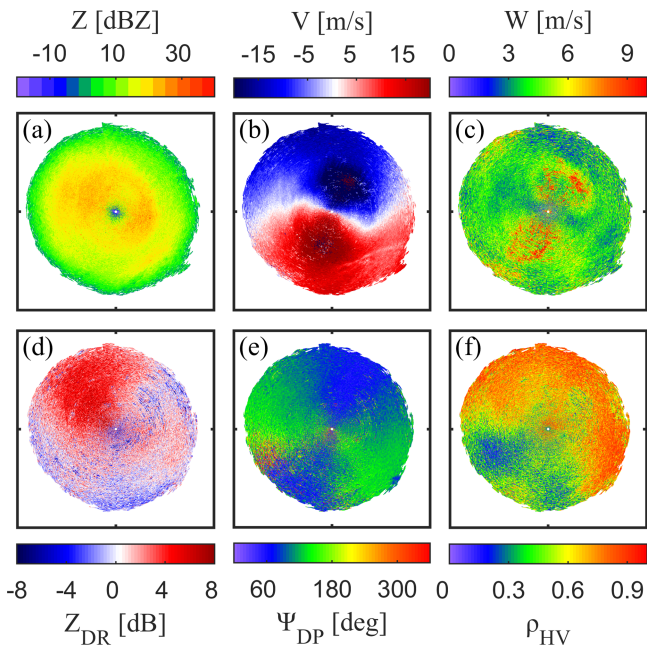


Fig. 2. Typical PPI image of migratory birds was recorded in Jinan city at 22:59, October 10, 2021 (UTC+8). Tiles cover a  $200 \text{ km} \times 200 \text{ km}$  square domain centered on the radar site. (a)  $Z$ . (b)  $V$ . (c)  $W$ . (d)  $Z_{DR}$ . (e)  $\Psi_{DP}$ . (f)  $\rho_{HV}$ .

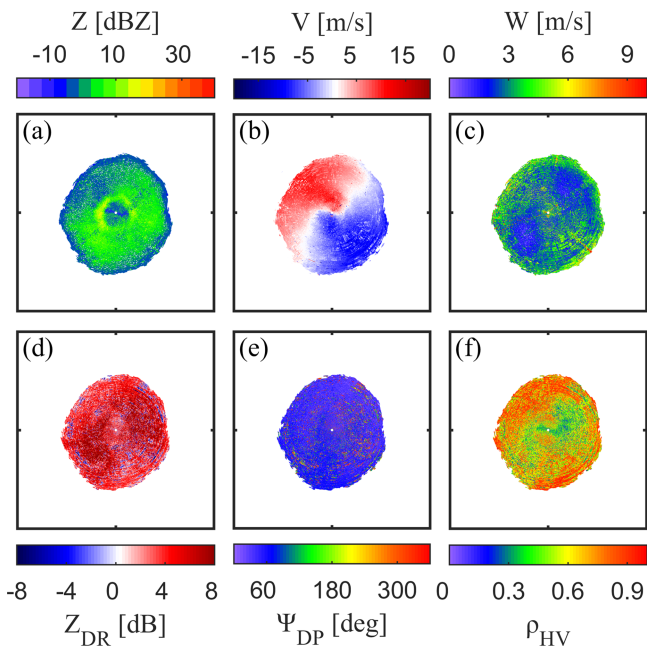


Fig. 3. Typical PPI image of migratory insects was recorded in Jinan city at 10:29, May 19, 2021 (UTC+8). Tiles cover a  $200 \text{ km} \times 200 \text{ km}$  square domain centered on the radar site. (a)  $Z$ . (b)  $V$ . (c)  $W$ . (d)  $Z_{DR}$ . (e)  $\Psi_{DP}$ . (f)  $\rho_{HV}$ .

testing the classifier due to its relatively large data size and few ground clutter. The polarimetric weather radar offers seven distinct product categories: reflectivity factor ( $Z$ ), radial velocity ( $V$ ), velocity spectrum width ( $W$ ), differential reflectivity factor ( $Z_{DR}$ ), differential phase shift ( $\Psi_{DP}$ ), differential phase shift ratio ( $K_{DP}$ ), and correlation coefficient ( $\rho_{HV}$ ). The gradient of

TABLE I  
MAIN TECHNICAL PARAMETERS OF THE BIRD RADAR

Specifications	
Frequency	Ku (16.01–17.018 GHz)
Max range	5 km
Blind area	200 m
Scan range	Azimuth: $0^\circ$ – $360^\circ$ , Elevation: $0^\circ$ – $40^\circ$
Resolution	Range: 15 m, Azimuth: $2.5^\circ$ , Elevation: $10^\circ$
Accuracy	Range: 10 m, Azimuth: $0.8^\circ$ , Elevation: $1^\circ$

$\Psi_{DP}$  over distance, known as  $K_{DP}$ , is not recorded by polarimetric weather radars when the  $\rho_{HV}$  is below 0.8. Consequently,  $K_{DP}$  was excluded from the dataset due to its notably smaller data size in comparison to other measurements. The use of  $Z$  is a source of controversy in classifying birds and insects, as it is simultaneously influenced by the size and density of targets within the radar beam. Despite birds having a significantly larger radar cross section (RCS) than insects, a high density of insects can lead to echo strength comparable to that of birds. Consequently, some researchers opted not to employ  $Z$  for the classification of birds and insects [24]. However, we conducted a manual examination of radar data from spring to fall 2021 at the Jinan site, revealing that the majority of insect echoes exhibit lower intensity than those of birds. As a result, we retained the use of  $Z$  in this article. Birds typically have stronger flight capabilities than insects, resulting in high values of  $V$  and  $W$  [11]. Insects are commonly wind-transported, leading to relatively lower values of  $V$  and  $W$  [11]. Thus, we employed  $V$  and  $W$  in this article. Furthermore, the dual-polarization moments, namely  $Z_{DR}$ ,  $\Psi_{DP}$ , and  $\rho_{HV}$ , were included in this article, as they are considered crucial elements for classifying birds and insects [24], [26]. Ultimately, all polarimetric weather radar moments except for the  $K_{DP}$  are chosen as inputs for the classifier.

### B. Bird Radar

The bird radar is situated atop the A-2 building at the Advanced Technology Research Institute of Beijing Institute of Technology in Jinan city, Shandong province, China ( $116^\circ 49' \text{ E}$ ,  $36^\circ 30' \text{ N}$ ). The bird radar is  $20^\circ$  south by the east of the polarimetric weather radar, and their straight-line distance is about 24 km, as shown in Fig. 1. The eastern side of the bird radar faces a wall, while its northern aspect is adjacent to a high-rise residential building. Consequently, the primary observation orientation of the bird radar is toward the west and south. The technical specifications of the bird radar are given in Table I.

The bird radar was capable of capturing flight trajectory data of targets and quantifying their density across various altitude layers [30]. In order to effectively detect both short-range and far-range targets, the bird radar employs alternating long and short pulses. Short pulses have a pulse width of  $1 \mu\text{s}$ . Their duty cycle time is  $15 \mu\text{s}$ , corresponding to a detection range of

200–2400 m. The pulse width of long pulses is 10  $\mu\text{s}$ , and the duty cycle time is 45  $\mu\text{s}$ . The corresponding detection range is 1500–5000 m.

The radar equation can be expressed as

$$P_r = \frac{P_t G^2 \lambda^2 \sigma}{(4\pi)^3 R^4} \quad (1)$$

where  $P_r$  is the received signal power,  $P_t$  is the averaged transmitted signal power,  $G$  is the antenna gain,  $\lambda$  is the wavelength of the signal,  $\sigma$  is the RCS of target,  $R$  is the distance between the target and the radar.

The  $P_t$  can be expressed as

$$P_t = P_p \tau f_p \quad (2)$$

where  $P_p$  is the peak power,  $\tau$  is pulse width, and  $f_p$  is repetition frequency.

According to the (2), the ratio of average transmitted power of long pulses and short pulses  $\rho_{LS}$  can be expressed as

$$\rho_{LS} = \frac{P_a^{\text{long}}}{P_a^{\text{short}}} = \frac{P_t \tau^{\text{long}} f_p}{P_t \tau^{\text{short}} f_p} = 10. \quad (3)$$

The bird radar calibration experiments revealed that the signal-to-noise ratio (SNR) of the echo from an unmanned aerial vehicle (DJI Phantom 4, RCS  $\sim 0.03 \text{ m}^2$ ) at 5 km is approximately 17 dB. Furthermore, we also adopted a detection threshold of 17 dB for the subsequent joint observation experiments.

As per (1), under constant radar system conditions, the SNR is determined by the target's RCS  $\sigma$  and its distance  $R$ . It is assumed that the RCS of insects in the Ku band is  $100 \text{ mm}^2$  [31]. According to (4), the maximum detection range of insect targets for long pulses is approximately 1.2 km. The blind area for the long pulse pattern of the bird radar extends to 1.5 km. Consequently, the bird radar is unable to detect insect targets using the long pulse pattern

$$R_{\text{max}}^{\text{long}} = \left( \frac{\sigma_{\text{insect}} R_{\text{UAV}}^4}{\sigma_{\text{UAV}}} \right)^{1/4} \approx 1.2 \text{ km}. \quad (4)$$

The distance from the short pulse of the bird radar to detect 17 dB SNR echo signal is about 2.8 km according to the (1) and (3). According to the (5), the max detection range of insect targets using short pulse pattern is about 0.673 km

$$R_{\text{max}}^{\text{short}} = \left( \frac{\sigma_{\text{insect}} R_{\text{UAV}}^4}{\sigma_{\text{UAV}}} \right)^{1/4} \approx 0.673 \text{ km}. \quad (5)$$

The max height is equal to the max range multiply the max elevation angle, as

$$H_{\text{max}}^{\text{short}} = R_{\text{max}}^{\text{short}} \times \sin(40^\circ) \approx 0.433 \text{ km}. \quad (6)$$

Nevertheless, only data within the altitude range of 0.64 km to 1.5 km is employed for this article, ensuring the accuracy of the bird density derived from the bird radar. The bird radar data collected between October 7 and 15, 2021, as well as from April 14 to June 25, 2022, are utilized to validate the weather radar approach for bird and insect classification.

### III. BIOLOGICAL SCATTERERS CLASSIFICATION METHOD

The process flow for polarimetric weather radar data is depicted in Fig. 4, encompassing data annotation and cleaning, point feature extraction, and classifier training. Data annotation and cleaning involve manual labeling of radar data and the removal of clutter. Point feature extraction entails computing spatial textures from the six input moments; subsequently, the resultant twelve one-dimensional (1-D) point features (six moments and their texture) are integrated into 12-D vectors. Finally, the feature vectors are used to training the classifier.

#### A. Data Annotation and Cleaning

The original radar moments are stored in polar coordinates, encompassing range bins, azimuth angles, elevation angles, and more. We select data in the first 400 range bins to generate a polar coordinate image. The image is subsequently projected onto rectangular coordinates using (7), resulting in a radar image of  $320 \times 320$  resolution achieved via linear interpolation.  $n$  our radar image, the  $X$ -axis signifies the east–west direction, while the  $Y$ -axis corresponds to the north–south direction; the radar is positioned at the image's center

$$\begin{cases} x = r \times \cos(\theta) \\ y = r \times \sin(\theta) \end{cases} \quad (7)$$

where  $r$  is the range bins,  $\theta$  is the azimuth angles,  $x$  and  $y$  are the detection range of radar in rectangular coordinates.

Subsequently, we employ EIsseg for manual annotation of radar images [32]. In particular, the manually delineated markers outline of radar echoes are multiplied with the binarized radar image masks to generate the final label images, depicted in Fig. 5.

After labeling the radar images, the challenge of eliminating clutter within the radar image persists, involving both ground clutter and precipitation. As ground clutter remains relatively constant over time, we analyzed radar images from November 2021 that lacked biological scatterers, and identified the absence of ground clutter, likely owing to the  $2.4^\circ$  elevation angle. Therefore, the ground clutter is negligible in this article. The echo intensity and polarization characteristics of precipitations differ significantly from those of biological scatterers, enabling straightforward labeling and removal during dataset creation. Ultimately, radar images that have been annotated and cleansed are utilized to construct the weather radar dataset for migration birds and insects.

#### B. Point Feature Extraction

Apart from the radar moments themselves, we are also intrigued by the texture features in these radar images. Prior research commonly computed the texture of moments within polar coordinates (range  $\times$  azimuth) [23], [24], [33]. However, the dimensions of the range  $\times$  azimuth windows vary across distinct range segments, leading to discrepancies and introducing errors in the texture features of moments. Hence, the calculation of moment textures in this article is undertaken within rectangular

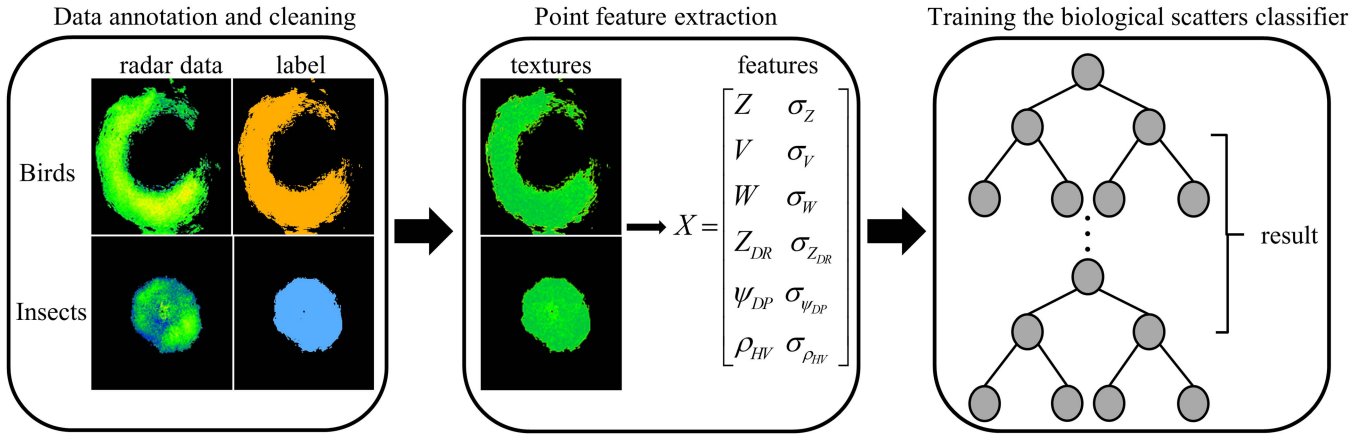


Fig. 4. Flowchart of the process of the biological scatter classifier training.

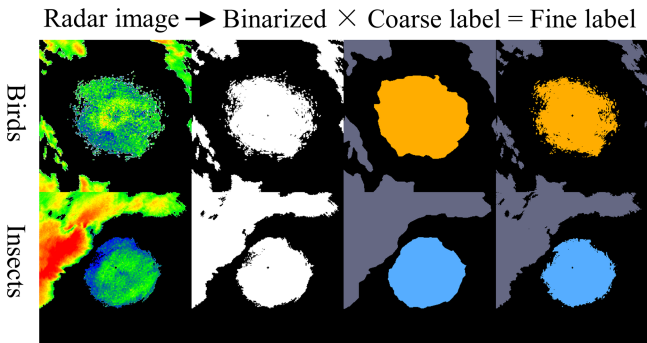


Fig. 5. Process of fine annotation of radar images. The orange, blue, and gray color represent the label of birds, insects, and precipitations, respectively.

coordinates, as follows:

$$\Delta m_{x,y} = \frac{1}{N-1} \sum_{i=-2}^2 \sum_{j=-2}^2 |m_{x,y} - m_{x+i,y+j}| \quad (8)$$

where the  $m$  is the radar moment,  $x$  and  $y$  are the radar detection range in rectangular coordinates,  $i$  is the  $x$  offset,  $j$  is the  $y$  offset,  $N$  is the window size. In this article, the  $N$  equals to  $5 \times 5$ .

At last, the six 1-D moments and six 1-D textures are combined into a 12-D feature vector  $X$ , which can be expressed as

$$X = \begin{bmatrix} Z, V, W, Z_{DR}, \phi_{DP}, \rho_{HV} \\ \sigma_Z, \sigma_V, \sigma_W, \sigma_{Z_{DR}}, \sigma_{\phi_{DP}}, \sigma_{\rho_{HV}} \end{bmatrix} \quad (9)$$

where  $\sigma$  is the texture of moments.

### C. Biological Scatter Classifier Training

The random forest algorithm [34] has found broad applications across various domains, including remote sensing [35], text recognition [36], image classification [37], financial prediction [38], and medical diagnosis [39], owing to its notable classification efficacy and noise resilience. Moreover, the random forest algorithm has demonstrated successful applications in the realm of weather radar, particularly for tasks such as quantitative

TABLE II  
CONFUSION MATRIX FOR CLASSIFYING BIRDS AND INSECTS

Classifier output \ True label	Bird	Insects
Bird	$TP$	$FP$
Insects	$FN$	$TN$

precipitation estimation and precipitation type recognition [40], [41], [42], [43], [44]. In this article, we employed the random forest algorithm from the scikit-learn package in Python 3.9 to train and evaluate the biological scatter classifier. The resultant classifier was constructed using 100 trees [45].

From the dataset containing 4142 radar images, we extract samples while ensuring that the number of collected bird (insect) samples in each image does not surpass 5000. This measure is taken to mitigate the overall data volume. As a result, we acquire a total of ten million insect samples and six million bird samples from the dataset. To further curtail data volume, we randomly selected two million bird samples and two million insect samples for training and testing the classifier. Seventy percent of the samples were allocated to the training set, while the remaining 30% constituted the test set. K-fold cross-validation is employed to fine-tune the classifier's hyperparameters and prevent overfitting during the training process [46]. In this article, the training set is divided into five folds: four for training and one for validation. This division is repeated five times.

Table II gives the confusion matrix for our classification problem. The accuracy (ACC), true positive rate (TPR), and true negative rate (TNR) are used to evaluate the performance of the biological scatter classifier, and they are calculated as follows:

$$ACC = \frac{TP + TN}{TP + TN + FP + FN} \quad (10)$$

$$TPR = \frac{TP}{TP + FN} \quad (11)$$

$$TNR = \frac{TN}{TN + FP} \quad (12)$$

#### D. Bird Radar Data Validation Method

When weather radars detected biological scatters, we conducted a comparison with the monitoring outcomes of the bird radar. If the vertically integrated density (VID) of birds detected by the bird radar surpasses the threshold, the shared observational region of both weather radar and bird radar is designated as bird-dominant (truth-label = 1). Conversely, if the VID does not exceed the threshold, the shared observational airspace is categorized as insect-dominant (truth-label = -1). Finally, the classification labels produced by the biological scatter classifier from the weather radars are compared with the truth-labels, thus validating the classifier's accuracy.

The bird radar data must be temporally and spatially aligned with the polarimetric weather radar data for comparative analysis. The time-matching procedure involves selecting the commencement and termination times of the bird radar, corresponding to the initiation time of two adjacent PPIs from the weather radar. Subsequently, the bird density within this interval is calculated. The spatial matching approach entails identifying the shared airspace that can be concurrently observed by both radars. To streamline the spatial alignment of the two radars, we re-interpolate the classification outcomes (in rectangular coordinates) of the weather radar to polar coordinates. According to the relative positions of two radars and the maximum detection range of the bird radar, weather radars data within the 76th to 116th range gates with azimuth angles from  $150^\circ$  to  $180^\circ$  is statistics.

In the following way, the  $Z$  of weather radar needed to be converted to the vertically integrated reflectivity (VIR), which is widely used in aeroecology research [47]. The  $Z$  (dBZ) is transformed to reflectivity  $\eta$  ( $\text{cm}^2\text{km}^{-3}$ ) as follows [48]:

$$\eta [\text{dB}] = Z [\text{dBZ}] + \beta \quad (13)$$

$$\beta = 10 \log_{10} \left( 10^3 \pi^5 |K_m|^2 / \lambda^4 \right) \quad (14)$$

$$|K_m|^2 = \left| \frac{m^2 - 1}{m^2 + 2} \right|^2 \quad (15)$$

$$\eta [\text{cm}^2\text{km}^{-3}] = 10^{\eta[\text{dB}]/10} \quad (16)$$

where  $Z$  is the reflectivity factor,  $\eta$  is the reflectivity,  $m$  is the complex refractive index of the animal ( $|K_m|^2 = 0.93$  for liquid water at C-band and S-band) [47], and  $\lambda \approx 10.6$  cm is the wavelength of weather radars. VIR can be obtained by integrating the  $\eta$  at different azimuth and range gates.

Weather radars operate in the volume PPI scan mode, while the bird radar employs the volume range height indicator scan mode. Thus, confirming the classification outcomes pixel by pixel within the joint observational region of the two radars presents significant challenges. Validating the averaged echo types across the entire region emerges as a feasible approach. The weather radars' approach involves comparing the VIR of birds and insects, with the higher value determining the representative label for the entire region.

The  $2.4^\circ$  elevation PPI's beam height ranges from 0.64 to 1.5 km across the 76th to 116th range gates. Consequently, the bird radar calculates the bird density within the height interval

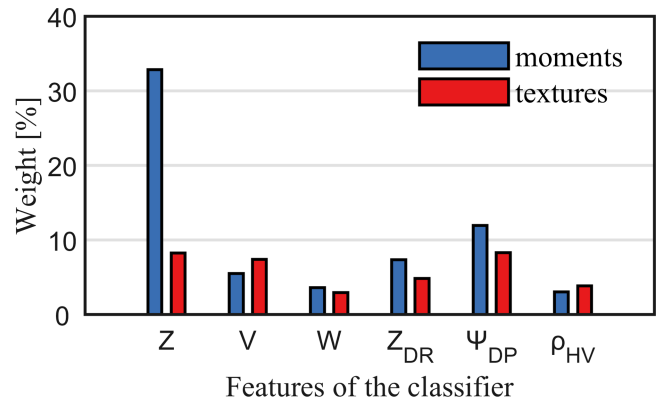


Fig. 6. Importance of features in the biological scatter classifier. Blue bars represent the moments and red bars represent the textures of moments.

of 0.64~1.5 km and integrates it to determine the VID. The threshold of VID for classifying birds and insects using bird radar is selected by the receiver operating characteristic (ROC) curve, it will be examined in the result section.

## IV. RESULT

The testing set comprised 300 000 bird samples and 300 000 insect samples. Five typical cases of migration bird and insects are tested to verify the performance of the biological scatter classifier. In addition, weather radar data from the Jinan site for October 2021 and the period of April to June 2022 were chosen to validate the classifier's outcomes using the joint observation data from the bird radar.

### A. Weather Radar Dataset Evaluation

After the completion of classifier training, the averaged ACC of the 5-fold cross validation method is 93.54%. All 600 000 samples of the testing set are tested, and the ACC = 93.56%, the TPR = 93.82%, and the TNR = 93.30%.

Feature importance was derived using the `feature_importances_` function from the sklearn library in Python 3.9 [45], as illustrated in Fig. 6. Notably,  $Z$  exerts the most substantial influence on the classifier, with a weight of 32.83%. The significance of  $\Psi_{DP}$  ranks second only to  $Z$ , with a value of 11.96%. Following  $\Psi_{DP}$ , the third and fourth positions are occupied by the importance of  $\Psi_{DP}$ 's texture and  $Z$ 's texture, with values of 8.32% and 8.26%, respectively. The influence of  $Z_{DR}$  and  $V$ 's texture is closely matched, at 7.36% and 7.40%, respectively.  $V$ 's importance also exceeds 5%. For the remaining features, their weight remains under 5%, encompassing  $W$ ,  $W$ 's texture,  $Z_{DR}$ 's texture,  $\rho_{HV}$ , and  $\rho_{HV}$ 's texture.

Finally, five representative scenarios are examined to validate the precision of the biological scatter classifier. These scenarios encompass two instances of bird migration, two instances of insect migration, and a scenario involving the concurrent migration of birds and insects. Furthermore, the observational data from the bird radar is employed to assess the accuracy of the classification outcomes for both birds and insects, utilizing the biological scatter classifier.

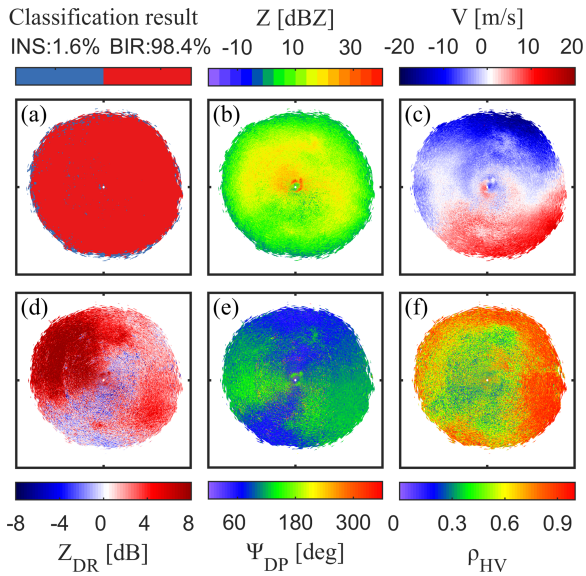


Fig. 7. Typical PPI image of migratory birds was recorded in Jinan city at 19:29 on September 22, 2021, Chinese standard time (UTC+8). Tiles cover a  $200 \text{ km} \times 200 \text{ km}$  square domain centered on the radar site. (a) Classification result of the biological scatter classifier. (b) Z. (c) V. (d)  $Z_{DR}$ . (e)  $\Psi_{DP}$ . (f)  $\rho_{HV}$ .

Fig. 7 illustrates the  $2.4^\circ$  elevation PPI image captured by the polarimetric weather radar at the Jinan site at 19:29 on September 22, 2021, in accordance with Chinese standard time (UTC+8). This instance exemplifies a typical case of bird migration. In Fig. 7(d)–(f), the  $Z_{DR}$ ,  $\Psi_{DP}$ , and  $\rho_{HV}$  each display notable azimuthal dependence. From the provided data, it can be deduced that the echoes in Fig. 7 are predominantly attributed to birds. The biological scatter classifier accurately identifies that bird-dominated range bins constitute 98.4% of this particular PPI, aligning with the manual assessment.

Fig. 8 displays the  $2.4^\circ$  elevation PPI image captured by the polarimetric weather radar at the Jinan site at 11:32 on May 20, 2021, in accordance with Chinese standard time (UTC+8). This instance represents a characteristic scenario of insect migration. The mean  $Z_{DR}$  value in Fig. 8(d) is notably high and exhibits little variation across azimuth angles. Given the provided data, it is evident that the echoes in Fig. 8 predominantly correspond to insects. The biological scatter classifier accurately identifies that insect-dominated range bins constitute 98.7% of this specific PPI, aligning with the manual assessment.

Generally, the Z value for birds is higher than that for insects [23], [26]. Nevertheless, there are instances where the Z value of birds may be lower than that of insects. Given that the Z value serves as a pivotal feature in the biological scatter classifier, distinguishing between low Z bird echoes and high Z insect echoes poses a challenge. To assess the performance of the biological scatter classifier, tests were conducted involving a scenario of low Z bird echoes and another with high Z insect echoes. Fig. 9 presents the  $2.4^\circ$  elevation PPI image obtained from the polarimetric weather radar at the Jinan site at 13:31 on July 4, 2021, based on Chinese standard time (UTC+8). This instance represents a characteristic example of the high Z insect scenario. The mean Z value in Fig. 9(b) amounts to 3.9 dBZ.

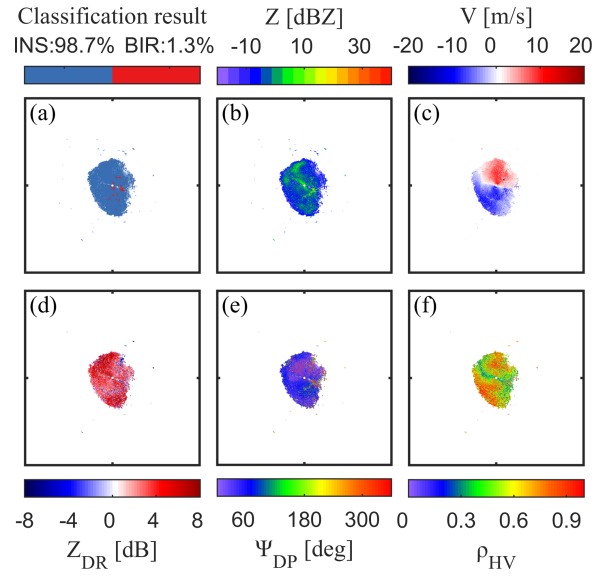


Fig. 8. Typical PPI image of migratory insects was recorded in Jinan city at 19:32 on May 20, 2021, Chinese standard time (UTC+8). Tiles cover a  $200 \text{ km} \times 200 \text{ km}$  square domain centered on the radar site. (a) Classification result of the biological scatter classifier. (b) Z. (c) V. (d)  $Z_{DR}$ . (e)  $\Psi_{DP}$ . (f)  $\rho_{HV}$ .

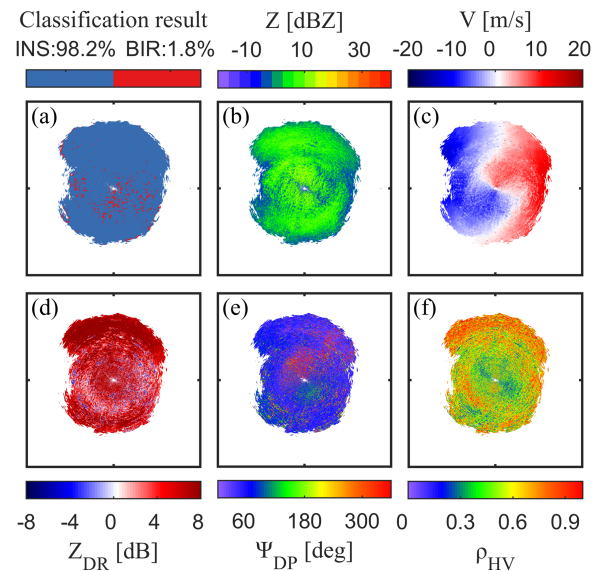


Fig. 9. Typical PPI image of strong insect migration cases was recorded in Jinan city at 13:31 on July 4, 2021, Chinese standard time (UTC+8). Tiles cover a  $200 \text{ km} \times 200 \text{ km}$  square domain centered on the radar site. (a) Classification result of the biological scatter classifier. (b) Z. (c) V. (d)  $Z_{DR}$ . (e)  $\Psi_{DP}$ . (f)  $\rho_{HV}$ .

Fig. 10 depicts the  $2.4^\circ$  elevation PPI image captured by the polarimetric weather radar at the Jinan site at 05:29 on April 6, 2021, in accordance with Chinese standard time (UTC+8). This situation typifies a scenario of low Z bird echoes. The mean Z value in Fig. 10(b) is recorded as 0.49 dBZ. The mean Z value in Fig. 9(b) surpasses that in Fig. 10(b). The biological scatter classifier accurately identifies 98.2% insect-dominated range bins in Fig. 9 and 87.4% bird-dominated range bins in Fig. 10, aligning with the manual assessment.

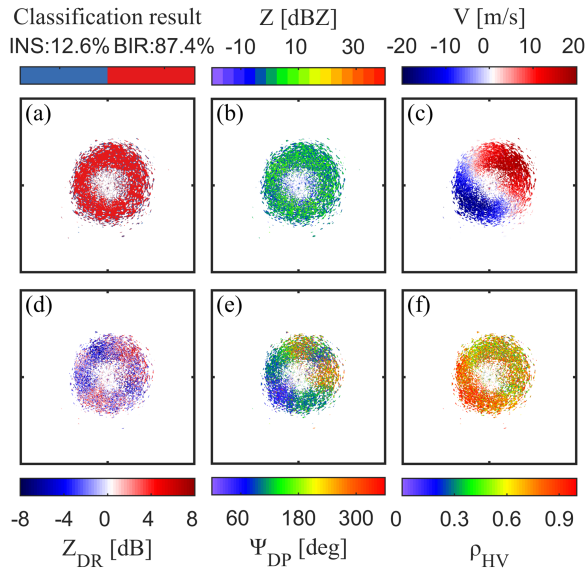


Fig. 10. Typical PPI image of migratory birds was recorded in Jinan city at 05:29 on April 6, 2021, Chinese standard time (UTC+8). Tiles cover a  $200 \text{ km} \times 200 \text{ km}$  square domain centered on the radar site. (a) Classification result of the biological scatter classifier. (b)  $Z$ . (c)  $V$ . (d)  $Z_{DR}$ . (e)  $\Psi_{DP}$ . (f)  $\rho_{HV}$ .

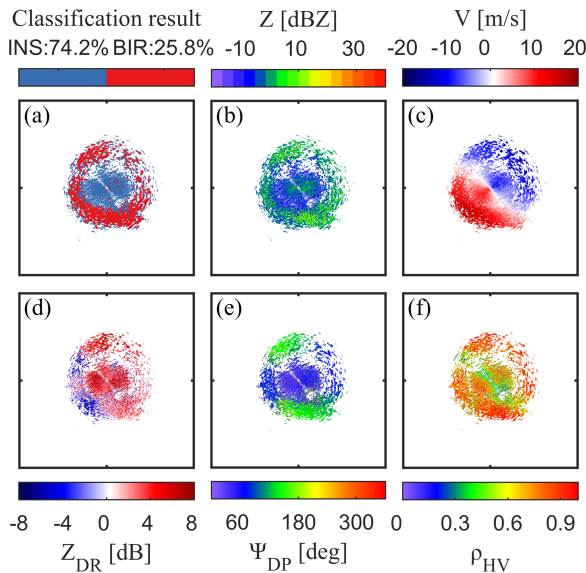


Fig. 11. A typical PPI image of migratory mixed cases of birds and insects was recorded in Jinan city at 12:00 on October 19, 2021, Chinese standard time (UTC+8). Tiles cover a  $200 \text{ km} \times 200 \text{ km}$  square domain centered on the radar site. (a) the classification result of the biological scatter classifier. (b)  $Z$ . (c)  $V$ . (d)  $Z_{DR}$ . (e)  $\Psi_{DP}$ . (f)  $\rho_{HV}$ .

Fig. 11 displays the  $2.4^\circ$  elevation PPI scan captured by the polarimetric weather radar at the Jinan site precisely at 12:00 on October 19, 2021, in accordance with Chinese Standard Time (UTC+8). This instance serves as a prototypical scenario, showcasing the concurrent presence of bird and insect targets. The echoes within this PPI can be categorized into two regions: circular echoes centered around the radar site and annular echoes extending beyond the circular region. The average  $Z_{DR}$  values of circle echoes and annular echoes is 3.0 and 0.88 dB, respectively.

In addition, the  $Z_{DR}$  and  $\Psi_{DP}$  for annular echoes display substantial azimuthal variability, whereas circular echoes do not. The data provided suggests that insects are the predominant source of circular echoes, while birds dominate the annular echoes. The biological scatter classifier precisely distinguished between range bins dominated by birds and insects, aligning well with manual assessment.

### B. Bird Radar Data Validation

Figs. 12 and 13 depict the exported VIR and VID data from both weather radars and the bird radar, along with their corresponding labels. Evidently, the majority of bird VID and VIR exhibit heightened values during nocturnal hours (from sunset to sunrise), while insect VIR peaks during daytime. Moreover, in situations with sparse migratory bird activity, insect VIR values remain comparable between day and night. The biological scatter classifier's performance is assessed using the ACC, TPR, and TNR metrics, which are derived by contrasting labels from the two radars (with labels from the bird radar considered as the ground truth). The ACC attains 95.36% (based on 6372 samples), while the TPR and TNR achieve 95.51% (from 2880 samples) and 95.24% (from 3492 samples) respectively. All three metrics, ACC, TPR, and TNR, surpass the 95% threshold, thus demonstrating the commendable efficacy of the biological scatter classifier. Various VID thresholds were tested to get the ROC curve, and the ACC reached its peak of 95.36% when the threshold was set at 11 dB, as depicted in Fig. 14. The ACC computed using the two radars is slightly greater than that derived from the weather radar's testing set. This discrepancy might arise due to the fact that it is based on the average label of the comprehensive joint observation (averaging across 1271 range bins).

## V. DISCUSSION

The method we propose is capable of classifying bird and insect migration within the PPI image of the polarimetric weather radar, achieving an accuracy rate of 93.56%. Furthermore, the suggested approach is adaptable to intricate scenarios, encompassing instances involving low  $Z$  bird cases, high  $Z$  insect cases, and scenarios characterized by the simultaneous mass migration of both birds and insects.

$Z$  holds the utmost significance as a feature in the biological scatter classifier, with a prominence of 32.83%. The biological scatter classifier demonstrates favorable performance in scenarios involving high  $Z$  insects (see Fig. 9, 98.2%), comparable to outcomes observed in low  $Z$  insect scenarios (see Fig. 8, 98.7%). Performance of the biological scatter classifier diminishes in cases of low  $Z$  birds (see Fig. 10, 87.4%) compared to high  $Z$  bird scenarios (see Fig. 7, 98.4%). The value of  $Z$  appears to exert little influence on insect identification but significantly impacts bird identification. However, instances of low  $Z$  bird cases generally manifest during the initiation and termination phases of migration, constituting a relatively small portion of the overall bird migration process. Consequently, their impact on migratory bird recognition is limited. In summary, the positive



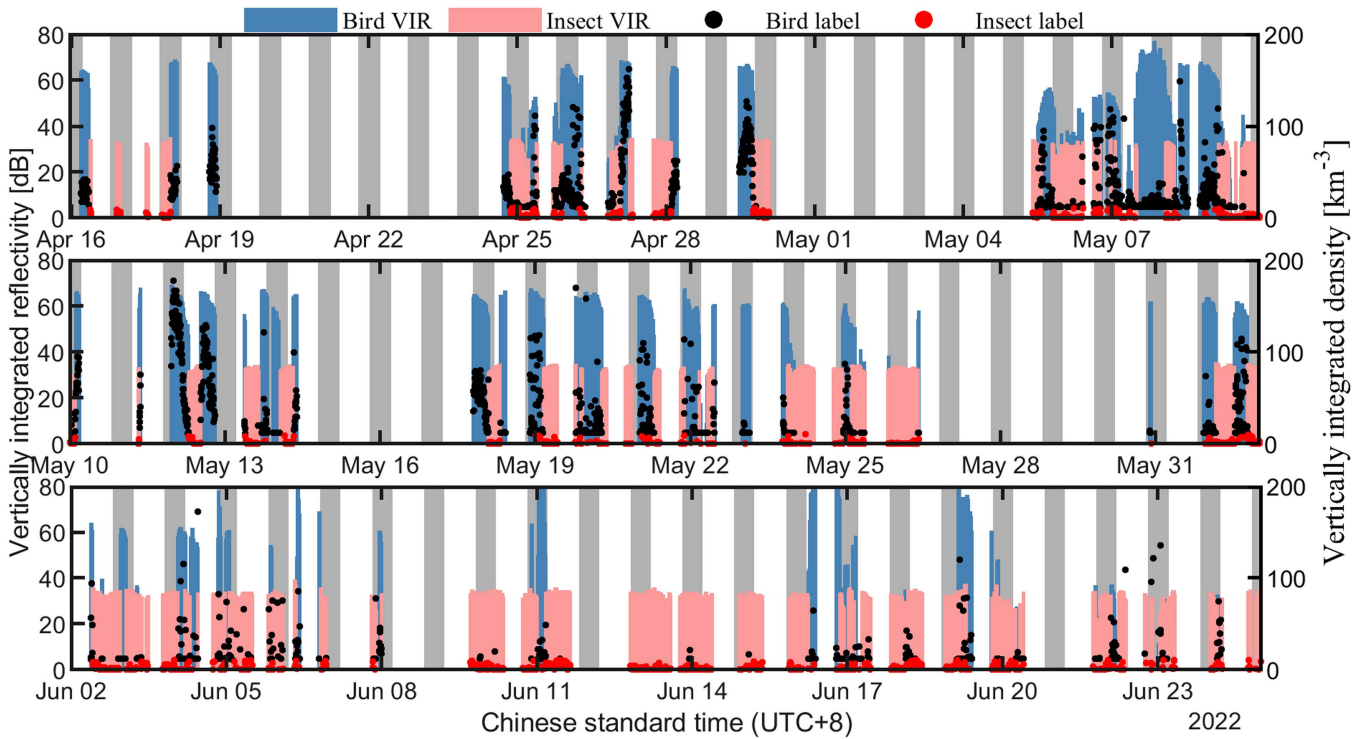


Fig. 12. Data was collected in April to June, 2022. The black and red color of points represents birds label and insects label, exported by the bird radar, respectively, and their height represents the size of the VID of birds. The blue and pink colors represent the predicted label of bird and insect output by the biological scatter classifier, and the height of columns represents the size of VIR retrieved by weather radars. Grey-shaded areas represent nighttime. Some of the missing data is due to rain, or the bird radar did not work.

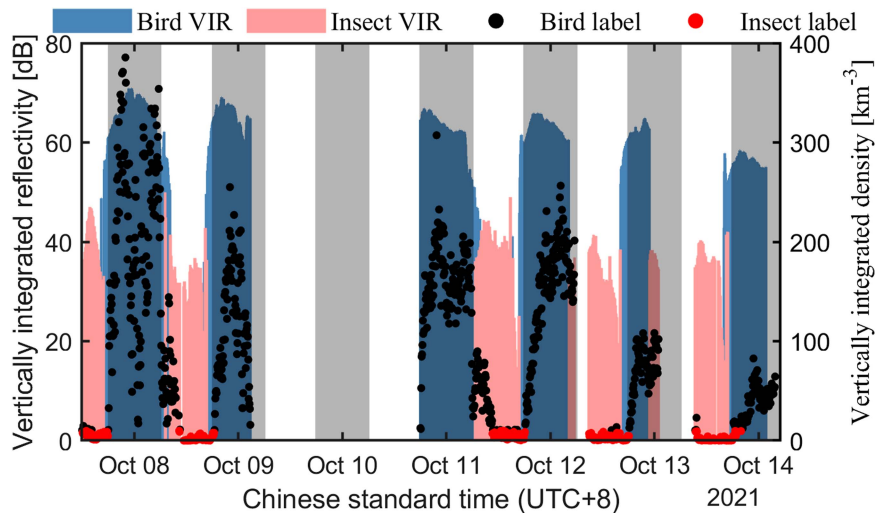


Fig. 13. Data was collected in October, 2021. The black and red color of points represents birds label and insects label, exported by the bird radar, respectively, and their height represents the size of the VID of birds. The blue and pink colors represent the predicted label of birds and insect output by the biological scatter classifier, and the height of columns represents the size of VIR retrieved by weather radars. Grey-shaded areas represent nighttime. Some of the missing data is due to rain, or the bird radar did not work.

impact of  $Z$  significantly outweighs any negative effects for classifying the migration of birds and insects using CINRAD.

The  $\Psi_{DP}$  constitutes the second most important feature in the biological scatter classifier, accounting for 11.96% significance. Morphological features of  $\Psi_{DP}$  images during migration exhibit consistency across seasons, displaying pronounced azimuthal

symmetry along the orientation axis, as depicted in Figs. 7(e), 10(e), and 11(e). The  $\Psi_{DP}$  values at the heads and tails of migratory birds are low, comparable to those of insects. Conversely, the  $\Psi_{DP}$  of the lateral body sections of migratory birds exceeds that of insects, offering valuable cues for differentiating between bird and insect.

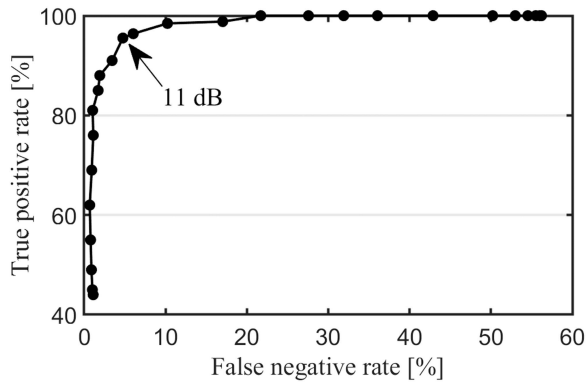


Fig. 14. ROC curve of the biological scatter classifier using different VID thresholds.

In contrast to earlier studies [24], [26], the significance of  $Z_{DR}$  within the biological scatter classifier is modest, securing the fifth position among all features—ranking below  $Z$ ,  $\Psi_{DP}$ ,  $Z$  texture, and  $\Psi_{DP}$  texture. Certain researchers have observed that the asymmetries in  $Z_{DR}$  of bird echoes maintain consistency throughout a migratory season, yet exhibit substantial variations among distinct radar locations. This observation further points out that the asymmetries of  $Z_{DR}$  are the result of the radar system’s transmission phase or frequency [29]. The phenomenon of  $Z_{DR}$  asymmetries is similarly prevalent in our bird dataset samples, as demonstrated in Fig. 7(d). Consequently, the presence of bird samples with high  $Z_{DR}$  levels diminishes the relevance of  $Z_{DR}$  within the biological scatter classifier.

$V$  (5.5%) and  $W$  (3.6%) exhibit lower significance compared to  $Z$ ,  $Z_{DR}$ , and  $\Psi_{DP}$ , yet hold greater weight than  $\rho_{HV}$  (3.1%). The  $\rho_{HV}$  serves as a valuable attribute for differentiating between biological scatters and precipitation. Nonetheless, the  $\rho_{HV}$  values for both birds and insects remain low due to their non-spherical shapes. Consequently, utilizing  $\rho_{HV}$  as a means of distinguishing between birds and insects proves challenging. Birds typically possess greater flying capabilities than insects, resulting in higher airspeeds. However, weather radar solely captures the radial velocity of target ground speed, contingent on factors such as wind speed, wind direction, airspeed of targets, and the angle between the target’s movement direction and the radar beam’s orientation. These factors collectively impact the significance of  $V$  in distinguishing between birds and insects.  $W$  relies on the standard deviation of radial velocity among targets encompassed within the radar beam. Consequently, actively flying birds typically exhibit higher  $W$  values compared to their passively flying insect counterparts. Nevertheless, the significance of  $W$  (3.6%) ranks lower than that of other moments except for  $\rho_{HV}$ . This could be attributed to  $W$ ’s susceptibility to considerable noise interference. Furthermore, atmospheric turbulence could also impact the  $W$  values.

The texture of moments also assumes a pivotal role in the classification of birds and insects. The cumulative weight of the six texture features amounts to 35.65%, surpassing that of the most significant feature,  $Z$ . The texture of  $\Psi_{DP}$ ,  $Z$ , and  $V$  exhibits relatively substantial weights: 8.32%; 8.26%; and 7.40%, respectively. Notably, the significance of the texture of  $V$  surpasses that of  $V$  itself. Prior research also employed the

texture of dual-polarization moments for the classification of birds and insects, and they determined that the impact of textures on bird and insect classification is inconspicuous [24]. This could be attributed to their calculation of moment textures under polar coordinates, resulting in errors due to variations in the area of the range  $\times$  azimuth windows across different range bins.

The proposed method can also be applied to radar data at different elevation angles, such as 0.5°, 1.5°, 2.4°, 3.4°, and 4.3°. However, we do not recommend using a biological scatter classifier trained with one elevation angle, such as 2.4°, to classify data from other elevation angles, such as 0.5°, 1.5°, and so on. The observation angle and coverage height range of radar beams at different elevation angles vary, resulting in slight differences in target scatter properties, which may decrease classifier performance. It is preferable to train the biological scatter classifier and classify biological scatters using the same elevation angle data. Training a universal classifier with data from all five elevation angles is also feasible, but it may require more complex methods, such as deep neural networks, to handle the diverse features of different elevation radar data.

## VI. CONCLUSION

We trained a biological scatter classifier by extracting point features and spatial texture features from 4142 polarimetric weather radar images, achieving an ACC of 93.56%. Our analysis identified  $Z$  as the pivotal moment for bird and insect classification, with a weight of 32.83%. Dual-polarization moments, namely  $\Psi_{DP}$  and  $Z_{DR}$ , also exert influence on the biological scatter classifier’s performance, carrying weights of 11.96% and 7.36%, respectively. Conversely,  $V$ ,  $W$ , and  $\rho_{HV}$  have a relatively limited impact on classifier performance, with weights of 5.53%, 3.60%, and 3.07%, respectively. Furthermore, moment textures play a significant role in the classifier, collectively weighing 35.65%, surpassing the most influential feature,  $Z$ . In addition, a bird radar is employed to validate and assess the biological scatter classifier’s accuracy. The labels determined by the bird radar serve as the ground truth for comparison against the labels generated by the biological scatter classifier. This validation yields an ACC of 95.36%, a TPR of 95.51%, and a TNR of 95.24%, thus affirming the classifier’s precision.

Currently, a limitation exists due to the indirect nature of the method used for verifying insect echoes. We intend to establish a vertical-looking insect radar at the Advanced Technology Research Institute of Beijing Institute of Technology, situated in Jinan city, Shandong province, China. This radar will validate the accuracy of the biological scatter classifier in identifying insect echoes. Concerning algorithms, we aim to enhance the performance of the biological scatter classifier at two levels: radar moments and radar spectrum. At the radar moments level, the proposed method only considers features within individual range bins and their immediate neighborhoods, neglecting features at broader scales. We intend to employ deep neural networks to extract multiscale features from radar scans, thereby enhancing the performance of the biological scatter classifier. At the radar spectrum data level, we intend to utilize spectrum data processing technology for classifying bird, insect, precipitation, and other echoes within individual range bins.

## ACKNOWLEDGMENT

The authors thank the Meteorological Observation Center, China Meteorological Administration, Beijing, China, for providing weather radar data. They would also like to thank the Key Laboratory for Meteorological Disaster Prevention and Mitigation of Shandong Province, Jinan, China, and Shandong Institute of Meteorological Sciences, Jinan, China.

## REFERENCES

- [1] S. Bauer and B. J. Hoyer, "Migratory animals couple biodiversity and ecosystem functioning worldwide," *Science*, vol. 344, no. 6179, Apr. 2014, Art. no. 1242552.
- [2] G. Hu et al., "Mass seasonal bioflows of high-flying insect migrants," *Science*, vol. 354, no. 6319, pp. 1584–1587, Dec. 2016.
- [3] D. L. Wagner, E. M. Gries, M. L. Forister, M. R. Berenbaum, and D. Stopak, "Insect decline in the anthropocene: Death by a thousand cuts," *Proc. Nat. Acad. Sci.*, vol. 118, no. 2, 2021, Art. no. e2023989118.
- [4] K. V. Rosenberg et al., "Decline of the North American avifauna," *Science*, vol. 366, no. 6461, pp. 120–124, 2019.
- [5] S. Altizer, R. Bartel, and B. A. Han, "Animal migration and infectious disease risk," *Science*, vol. 331, no. 6015, pp. 296–302, 2011.
- [6] S. A. Lambertucci, E. L. C. Shepard, and R. P. Wilson, "Human-wildlife conflicts in a crowded airspace," *Science*, vol. 348, no. 6234, pp. 502–504, 2015.
- [7] Q. Wu et al., "Migration patterns and winter population dynamics of rice planthoppers in Indochina: New perspectives from field surveys and atmospheric trajectories," *Agricultural Forest Meteorol.*, vol. 265, pp. 99–109, 2019.
- [8] J. Guo, X. Fu, S. Zhao, X. Shen, K. A. G. Wyckhuys, and K. Wu, "Long-term shifts in abundance of (migratory) crop-feeding and beneficial insect species in northeastern Asia," *J. Pest Sci.*, vol. 93, no. 2, pp. 583–594, 2020.
- [9] X. Fu, "Study on community structure and population dynamics of migratory insects in the bohai bay," *Doctor. Chin. Acad. Agricultural Sci.*, 2015.
- [10] G. Boere and D. Stroud, "The flyway concept: What it is and what it isn't," pp. 40–47, 2006.
- [11] A. M. Dokter, F. Liechti, H. Stark, L. Delobbe, P. Tabary, and I. Holleman, "Bird migration flight altitudes studied by a network of operational weather radars," *J. Roy. Soc. Interface*, vol. 8, no. 54, pp. 30–43, 2011.
- [12] A. H. Sivakumar, D. Sheldon, K. Winner, C. S. Burt, and K. G. Horton, "A weather surveillance radar view of Alaskan avian migration," *Proc. Roy. Soc. B*, vol. 288, no. 1950, May 2021, Art. no. 20210232.
- [13] A. Dezfuli, K. G. Horton, B. Zuckerberg, S. D. Schubert, and M. G. Bosilovich, "Continental patterns of bird migration linked to climate variability," *Bull. Amer. Meteorol. Soc.*, vol. 103, no. 2, pp. E536–E547, 2022.
- [14] K. G. Horton et al., "Phenology of nocturnal avian migration has shifted at the continental scale," *Nature Climate Change*, vol. 10, no. 1, pp. 63–68, 2019.
- [15] K. Cui, H. Cheng, and W. Rui, "Deep-learning-based extraction of the animal migration patterns from weather radar images," *Sci. China-Inf. Sci.*, vol. 63, 2020, Art. no. 140304.
- [16] T.-Y. Lin et al., "MistNet: Measuring historical bird migration in the US using archived weather radar data and convolutional neural networks," *Methods Ecol. Evol.*, vol. 10, no. 11, pp. 1908–1922, 2019.
- [17] S. RoyChowdhury, "Distinguishing weather phenomena from bird migration patterns in radar imagery," in *Proc. IEEE Conf. Comput. Vis. Pattern Recognit. Workshops*, 2016, pp. 10–17.
- [18] S. Wang, C. Hu, K. Cui, R. Wang, H. Mao, and D. Wu, "Animal migration patterns extraction based on atrous-gated CNN deep learning model," *Remote Sens.*, vol. 13, no. 24, 2021, Art. no. 4998.
- [19] M. Leskinen et al., "Pest insect immigration warning by an atmospheric dispersion model, weather radars and traps," *J. Appl. Ecol.*, vol. 135, no. 1/2, pp. 55–67, 2011.
- [20] E. K. Haas, F. A. L. Sorte, H. M. McCaslin, M. C. T. D. Belotti, and K. G. Horton, "The correlation between eBird community science and weather surveillance radar-based estimates of migration phenology," *Glob. Ecol. Biogeography*, vol. 31, no. 11, pp. 2219–2230, 2022.
- [21] R. Nussbaumer, B. Schmid, S. Bauer, and F. Liechti, "A Gaussian mixture model to separate birds and insects in single-polarization weather radar data," *Remote Sens.*, vol. 13, no. 10, 2021, Art. no. 1989.
- [22] I. Holleman, "Quality control and verification of weather radar wind profiles," *J. Atmospheric Ocean. Technol.*, vol. 22, no. 10, pp. 1541–1550, Oct. 2005.
- [23] P. M. Stepanian, K. G. Horton, V. M. Melnikov, D. S. Zrnić, and S. A. Gauthreaux Jr., "Dual-polarization radar products for biological applications," *Ecosphere*, vol. 7, no. 11, 2016, Art. no. e01539.
- [24] P. Jatau, V. Melnikov, and T.-Y. Yu, "A machine learning approach for classifying bird and insect radar echoes with S-band polarimetric weather radar," *J. Atmospheric Ocean. Technol.*, vol. 38, no. 10, pp. 1797–1812, 2021.
- [25] P. Jatau and V. Melnikov, "Classifying bird and insect radar echoes at s-band," in *Proc. 35th Conf. on Environ. Inf. Process. Technol.*, 2019, p. 830.
- [26] S. Gauthreaux and R. Diehl, "Discrimination of biological scatterers in polarimetric weather radar data: Opportunities and challenges," *Remote Sens.*, vol. 12, no. 3, p. 545, 2020.
- [27] C. Larson, "Hostile shores," *Science*, vol. 350, no. 6257, pp. 150–152, Oct. 2015.
- [28] Y. Zhou et al., "Long-term insect censuses capture progressive loss of ecosystem functioning in East Asia," *Sci. Adv.*, vol. 9, no. 5, 2023, Art. no. eade9341.
- [29] P. M. Stepanian and K. G. Horton, "Extracting migrant flight orientation profiles using polarimetric radar," *IEEE Trans. Geosci. Remote Sens.*, vol. 53, no. 12, pp. 6518–6528, Dec. 2015.
- [30] R. Wang, H. Mao, K. Cui, Z. Sun, C. Hu, and D. Wu, "Quantification of migration birds based on polarimetric weather radar," *Remote Sens.*, vol. 15, no. 19, 2023, Art. no. 4809.
- [31] S. Kong et al., "Insect multifrequency polarimetric radar cross section: Experimental results and analysis," *IEEE Trans. Geosci. Remote Sens.*, vol. 59, no. 8, pp. 6573–6585, Aug. 2021.
- [32] Y. L. Y. Hao et al., "EISeg: An efficient interactive segmentation tool based on PaddlePaddle," 2022, *arXiv:2210.08788*.
- [33] V. Chandrasekar, R. Keränen, S. Lim, and D. Moiseev, "Recent advances in classification of observations from dual polarization weather radars," *Atmospheric Res.*, vol. 119, pp. 97–111, Jan. 2013.
- [34] L. Breiman, "Random forests," *Mach. Learn.*, vol. 45, no. 1, pp. 5–32, Oct. 2001.
- [35] M. Belgiu and L. Drăguț, "Random forest in remote sensing: A review of applications and future directions," *Int. Soc. Photogramm. Remote Sens. J. Photogramm. Remote Sens.*, vol. 114, pp. 24–31, Apr. 2016.
- [36] R. P. Kaur, M. Kumar, and M. K. Jindal, "Newspaper text recognition of Gurumukhi script using random forest classifier," *Multimedia Tools Appl.*, vol. 79, no. 11, pp. 7435–7448, Mar. 2020.
- [37] B. Xu, Y. Ye, and L. Nie, "An improved random forest classifier for image classification," in *Proc. IEEE Int. Conf. Inf. Automat.*, 2012, pp. 795–800.
- [38] S. Joshi, R. Ramesh, and S. Tahsildar, "A bankruptcy prediction model using random forest," in *Proc. 2nd Int. Conf. Intell. Comput. Control Syst.*, 2018, pp. 1–6.
- [39] F. Yang, H.-Z. Wang, H. Mi, C.-D. Lin, and W.-W. Cai, "Using random forest for reliable classification and cost-sensitive learning for medical diagnosis," *BMC Bioinf.*, vol. 10, no. 1, pp. 1–14, Jan. 2009.
- [40] Y. Mao and A. Sorteberg, "Improving radar-based precipitation nowcasts with machine learning using an approach based on random forest," *Weather Forecasting*, vol. 35, no. 6, pp. 2461–2478, Dec. 2020.
- [41] P.-S. Yu, T.-C. Yang, S.-Y. Chen, C.-M. Kuo, and H.-W. Tseng, "Comparison of random forests and support vector machine for real-time radar-derived rainfall forecasting," *J. Hydrol.*, vol. 552, pp. 92–104, Sep. 2017.
- [42] B. L. Medina et al., "A random forest method to forecast downbursts based on dual-polarization radar signatures," *Remote Sens.*, vol. 11, no. 7, p. 826, 2019.
- [43] J. Orellana-Alvear, R. Célleri, R. Rollenbeck, and J. Bendix, "Optimization of x-band radar rainfall retrieval in the southern andes of Ecuador using a random forest model," *Remote Sens.*, vol. 11, no. 14, 2019, Art. no. 1632.
- [44] B.-C. Seo, "A data-driven approach for winter precipitation classification using weather radar and NWP Data," *Atmosphere*, vol. 11, no. 7, p. 701, 2020.
- [45] F. Pedregosa et al., "Scikit-learn: Machine learning in python," *J. Mach. Learn. Res.*, vol. 12, no. 85, pp. 2825–2830, 2011.
- [46] R. Kohavi, "A study of cross-validation and bootstrap for accuracy estimation and model selection," in *Proc. 14th Int. Joint Conf. Artif. Intell.*, 1995.
- [47] A. M. Dokter et al., "bioRad: Biological analysis and visualization of weather radar data," *Ecography*, vol. 42, no. 5, pp. 852–860, 2018.
- [48] P. B. Chilson, W. F. Frick, P. M. Stepanian, J. R. Shipley, T. H. Kunz, and J. F. Kelly, "Estimating animal densities in the atmosphere using weather radar: ToZor not toZ?," *Ecosphere*, vol. 3, no. 8, pp. 1–19, 2012.



**Cheng Hu** (Senior Member, IEEE) received the B.S. degree in electronic engineering from the National University of Defense Technology, Changsha, China, in 2003, and the Ph.D. degree in target detection and recognition from Beijing Institute of Technology, Beijing, China, in 2009.

He was a Visiting Research Associate with the University of Birmingham, Birmingham, U.K., for 15 months from 2006 to 2007. Since 2009, he has been with the School of Information and Electronics, BIT, where he was a Full Professor in 2014. He is currently the Vice Director of the Radar Technology Research Institute with BIT. He has authored more than 60 SCI-indexed journal articles and more than 100 conference articles. His main research interests include new concept synthetic aperture radar imaging, and the biological detection radar system and signal processing.



**Zhuoran Sun** was born in Zhangjiakou, Hebei, China, in 1996. He received the B.S. degree in electronic science and technology from Heilongjiang University, Harbin, China, in 2018 and the M.S. degree in optical engineering in 2021 from Beijing Institute of Technology, Beijing, China, where he is currently working toward the D.Eng. degree in electronic information with the School of Information and Electronics.

His research interests include machine learning in weather radar signal processing and radar

aeroecology.



**Kai Cui** received the B.S. degree in information engineering and the Ph.D. degree in information and communication engineering from the Beijing Institute of Technology, Beijing, China, in 2015 and 2021, respectively.

From 2021 to 2024, he was a Postdoctoral Researcher with the School of Computer Sciences, Beijing Institute of Technology. Since 2024, he has been an Assistant Professor with the School of Information and Electronics, Beijing Institute of Technology. His main research interests include weather radar signal

processing for biological detection, and weather radar aeroecology.

Dr. Cui was the recipient of the IET International Radar Conference Best Paper Award in 2023.



**Huafeng Mao** was born in Shaoxing, Zhejiang, China, in 1995. He received the B.S. degree in information engineering in 2018 from Beijing Institute of Technology, Beijing, China, where he is currently working toward the Ph.D. degree in information and communication engineering with the School of Information and Electronics.

His research interests include radar target detection and tracking, entomological radar signal processing, weather radar signal processing, and radar aeroecology.



**Rui Wang** was born in Taiyuan, Shanxi, China, in 1985. He received the B.S. degree in information engineering and the Ph.D. degree in information and communication engineering from Beijing Institute of Technology, Beijing, China, in 2009 and 2015, respectively.

From 2012 to 2013, he was a Visiting Scholar with the Mullard Space and Science Laboratory, University College London, London, U.K. From 2015 to 2017, he was a Post-Doctoral Researcher with the Department of Electronics Engineering, Tsinghua University, Beijing, China. From 2018 to 2023, he was an Associate Professor with the School of Electronic Engineering, Beijing Institute of Technology, and since 2023, he has been a Professor with the School of Information and Electronics, Beijing Institute of Technology. His research interests include bistatic synthetic aperture radar imaging, stepped-frequency radar signal processing, ISAR imaging, and entomological radar signal processing to extract insect biological parameters.

Dr. Wang was the recipient of the IEEE CIE International Radar Conference Excellent Paper Award in 2011.



**Xiao Kou** was born in 1998 in Xi'an, Shaanxi Province, China. She received the bachelor's degree in electronic information engineering from Central South University, Changsha, China, in 2020. She is currently working toward the master's degree in information and communication engineering with the School of Information and Electronics, Beijing Institute of Technology, Beijing, China.

Her research interest covers radar signal processing and electromagnetic simulation.



**Dongli Wu** received the Ph.D. degree in ecology from Beijing Normal University, Beijing, China, in July 2007.

Since September 2009, she has been with the Meteorological Observation Center, CMA, Beijing, China, and promoted to be a Full Professor/Doctoral Supervisor and the Director of Ecology and Environment at the Meteorological Observation Technology Innovation Team, since 2018. She has authored or coauthored more than 20 journal articles. Her research interests include weather radar application,

agricultural meteorological observation technology, and automatic soil moisture observation.



**Fan Xia** received the master's degree in atmospheric sciences from Chengdu University of Information and Technology, Sichuan, China, in 2012.

Since 2012, he has been with the Shandong Meteorological Scientific Institution, Shandong, and promoted to be a Senior Engineer since 2020. She has authored or coauthored nearly ten journal articles. Her research interests include weather radar data processing and application, severe convection weather analysis, and mesoscale numerical forecasting simulation.